

## Article

# Synthesis of FeOOH-Loaded Aminated Polyacrylonitrile Fiber for Simultaneous Removal of Phenylphosphonic Acid and Phosphate from Aqueous Solution

Rui Zhou <sup>1,2,†</sup>, Wusong Xu <sup>1,2,†</sup>, Peisen Liu <sup>1,2</sup>, Shangyuan Zhao <sup>1,2</sup>, Gang Xu <sup>1,2,\*</sup> , Qizhong Xiong <sup>1,2</sup>, Weifeng Zhang <sup>1,2</sup> , Chaochun Zhang <sup>1,2</sup> and Xinxin Ye <sup>1,2</sup>

<sup>1</sup> Anhui Province Key Lab of Farmland Ecological Conservation and Pollution Prevention, Engineering and Technology Research Center of Intelligent Manufacture and Efficient Utilization of Green Phosphorus Fertilizer of Anhui Province, College of Resources and Environment, Anhui Agricultural University, Hefei 230036, China

<sup>2</sup> Key Laboratory of JiangHuai Arable Land Resources Protection and Eco-Restoration, Ministry of Natural Resources, College of Resources and Environment, Anhui Agricultural University, Hefei 230036, China

\* Correspondence: gangxu@ahau.edu.cn

† These authors contributed equally to this work.

**Abstract:** Phosphorus is one of the important metabolic elements for living organisms, but excess phosphorus in water can lead to eutrophication. At present, the removal of phosphorus in water bodies mainly focuses on inorganic phosphorus, while there is still a lack of research on the removal of organic phosphorus (OP). Therefore, the degradation of OP and synchronous recovery of the produced inorganic phosphorus has important significance for the reuse of OP resources and the prevention of water eutrophication. Herein, a novel FeOOH-loaded aminated polyacrylonitrile fiber (PAN<sub>A</sub>F-FeOOH) was constructed to enhance the removal of OP and phosphate. Taking phenylphosphonic acid (PPOA) as an example, the results indicated that modification of the aminated fiber was beneficial to FeOOH fixation, and the PAN<sub>A</sub>F-FeOOH prepared with 0.3 mol L<sup>-1</sup> Fe(OH)<sub>3</sub> colloid had the best performance for OP degradation. The PAN<sub>A</sub>F-FeOOH efficiently activated peroxydisulfate (PDS) for the degradation of PPOA with a removal efficiency of 99%. Moreover, the PAN<sub>A</sub>F-FeOOH maintained high removal capacity for OP over five cycles as well as strong anti-interference in a coexisting ion system. In addition, the removal mechanism of PPOA by the PAN<sub>A</sub>F-FeOOH was mainly attributed to the enrichment effect of PPOA adsorption on the fiber surface's special microenvironment, which was more conducive to contact with SO<sub>4</sub>•<sup>-</sup> and •OH generated by PDS activation. Furthermore, the PAN<sub>A</sub>F-FeOOH prepared with 0.2 mol L<sup>-1</sup> Fe(OH)<sub>3</sub> colloid possessed excellent phosphate removal capacity with a maximal adsorption quantity of 9.92 mg P g<sup>-1</sup>. The adsorption kinetics and isotherms of the PAN<sub>A</sub>F-FeOOH for phosphate were best depicted by pseudo-quadratic kinetics and a Langmuir isotherm model, showing a monolayer chemisorption procedure. Additionally, the phosphate removal mechanism was mainly due to the strong binding force of iron and the electrostatic force of protonated amine on the PAN<sub>A</sub>F-FeOOH. In conclusion, this study provides evidence for PAN<sub>A</sub>F-FeOOH as a potential material for the degradation of OP and simultaneous recovery of phosphate.

**Keywords:** polyacrylonitrile fiber; FeOOH; activate peroxydisulfate; organic phosphorus; adsorption



**Citation:** Zhou, R.; Xu, W.; Liu, P.; Zhao, S.; Xu, G.; Xiong, Q.; Zhang, W.; Zhang, C.; Ye, X. Synthesis of FeOOH-Loaded Aminated Polyacrylonitrile Fiber for Simultaneous Removal of Phenylphosphonic Acid and Phosphate from Aqueous Solution. *Polymers* **2023**, *15*, 1918. <https://doi.org/10.3390/polym15081918>

Academic Editors: Valeria La Parola and Leonarda Liotta

Received: 26 March 2023

Revised: 12 April 2023

Accepted: 13 April 2023

Published: 17 April 2023



**Copyright:** © 2023 by the authors. Licensee MDPI, Basel, Switzerland. This article is an open access article distributed under the terms and conditions of the Creative Commons Attribution (CC BY) license (<https://creativecommons.org/licenses/by/4.0/>).

## 1. Introduction

Phosphorus (P) is one of the most important elements in the world. It exists in the cells of living organisms, maintains the growth of bones, and joins in almost all physiological and chemical conversions [1]. However, P emissions continue to increase with increasing industrial production and agricultural activities [2]. High concentrations of P (10 mg L<sup>-1</sup>) cause water eutrophication, leading to the excessive growth of algae and aquatic plants,

reducing dissolved oxygen levels in the water, and even threatening human safety [3]. Currently, there are still many waters in China that are eutrophic; for example, Chaohu Lake shows an average total phosphorus concentration of  $0.215 \text{ mg L}^{-1}$  [4]. Moreover, about 65% of European Atlantic coastal waters are eutrophic [5]. Furthermore, P resources are not renewable, and the worldwide phosphorus crisis has gradually attracted people's attention. Therefore, the removal and recovery of P from wastewater have important research significance.

At present, the recovery and utilization of P in wastewater mainly focus on inorganic phosphorus; however, few studies have reported on organic phosphorus (OP) resource recovery and utilization [6]. OP is one of the important forms of phosphorus in water and livestock wastewater is the major pollution source, accounting for about 10–65% of total phosphorus [7,8]. Furthermore, OP compounds are widely applied as pesticides, scale inhibitors, flame retardants, and plasticizers [9,10]. Ester organophosphorus is the main existing form of OP, which is often detected in water bodies and seriously threatens water safety and human health [11,12]. Hence, the recovery and recycling of OP from wastewater are of imminent importance. However, the direct recovery of organophosphorus in wastewater is difficult. Transforming OP into inorganic phosphorus is an effective way to achieve its recovery and utilization, which has become the focus of people's attention.

Advanced oxidation processes (AOPs) are regarded as being the most valuable technologies for persistent organic pollutant degradation [13–15]. Among them,  $\text{SO}_4^{\bullet-}$  is more conducive to the degradation of organic pollutants due to its higher selectivity, longer life cycle, and wider pH adaptability [16,17]. However, the generation rate of  $\text{SO}_4^{\bullet-}$  from peroxydisulfate (PDS) or peroxymonosulfate (PMS) is relatively slow. Hence, various methods, including light, heat, bases, and transition metals [18,19], have been successfully used to activate persulfate. Among them, iron-based materials are widely selected due to their advantages of low cost, convenient source, and high catalytic activity. Recently,  $\text{Fe}^0$  [20],  $\text{FeS}$  [21],  $\text{Fe}_2\text{O}_3$  [22], and  $\text{FeOOH}$  [23] have been used as potential catalysts for persulfate activation. Among them,  $\text{FeOOH}$  has been widely used in the water treatment field [23–25]. For example, Zhao et al. [23] prepared a ball-milled  $\alpha\text{-FeOOH}$ /biochar composite to catalyze persulfate degradation of phenol with a high efficiency of 100%. Although important progress has been made in the degradation of organic pollutants in water by activating persulfate with  $\text{FeOOH}$ ,  $\text{FeOOH}$  is difficult to recycle and easily causes secondary pollution. Different supports, such as silica gel, carbon material, MOF, etc., have been used to load  $\text{FeOOH}$  for solving the above problems with significant research progress [25–27]. However, some of these materials usually have deficits such as low modification degree, harsh preparation conditions, or high cost, which would restrict their actual application. As we all know, suitable support is a prerequisite for improving catalytic activity and stability [28]. Therefore, it is of great significance to exploit new support materials for the construction of a  $\text{FeOOH}$ -supported catalyst used to activate persulfate for catalytic degradation of OP.

Among all of the potential catalyst supports, fibers have attracted much attention due to their high stability, large specific surface area, prominent recyclability, and ease of surface modification and regulation [29]. Polyacrylonitrile fiber (PANF) is widely used in the textile industry, architecture, and people's daily lives. Furthermore, PANF is rich in cyano and ester groups, which can be easily converted into various functional groups [30]. Our previous work successfully constructed different functionalized PANFs for organic catalysis [31,32], heavy metal removal [33,34] and phosphate purification [35–37]. It was found that a specific microenvironment was formed between the functional moieties and polymer segments, the cooperative effect of which could change the interaction strength, thus accelerating the catalytic or adsorption performance. Nevertheless, using functionalized PANF for the degradation and recovery OP has rarely been reported. In addition,  $\text{FeOOH}$  has the characteristics of simultaneously activating persulfate to degrade organic pollutants and adsorbing inorganic phosphorus, hence it is theoretically feasible and of great significance to prepare PANF-supported  $\text{FeOOH}$  for simultaneous OP degradation and inorganic phosphorus recovery.

In this work, a novel polyacrylonitrile fiber loaded with FeOOH (PAN<sub>A</sub>F-FeOOH) was synthesized using the sol-gel method to activate PDS for PPOA degradation. Phenylphosphonic acid (PPOA), a typical OP compound used as an important industrial chemical, was selected as the model pollutant [11]. The PPOA degradation and phosphate adsorption abilities of PAN<sub>A</sub>F-FeOOH were evaluated, and the main factors affecting the degradation of PPOA and phosphate removal were studied. Furthermore, the degradation of PPOA and phosphate purification mechanisms by PAN<sub>A</sub>F-FeOOH are discussed. The stability and feasibility in practical application of the fiber were also evaluated by continuous flow tests and repeatability experiments.

## 2. Materials and Methods

### 2.1. Materials and Instruments

The polyacrylonitrile fiber (PANF, containing about 93% acrylonitrile) and the polyethyleneimine (PEI, Mw = 10,000) were purchased from Fushun Petrochemical Co., Ltd. (Fushan, China) and Shanghai Dibo Biotechnology Co., Ltd. (Shanghai, China), respectively. Phenylphosphonic acid (98%) and ferric nitrate (Fe(NO<sub>3</sub>)<sub>3</sub>·9H<sub>2</sub>O) were obtained from Shanghai Aladdin Biochemical Technology Co., Ltd (Shanghai, China). and Shanghai Maclean Biochemical Co., Ltd (Shanghai, China), respectively. Additional reagents used in this study are detailed in Section S1 of the supporting information. The characterization methods for the materials prepared in this experiment are described in Section S2 of the supporting information.

### 2.2. Preparation of FeOOH-Supported Polyacrylonitrile Fiber (PAN<sub>A</sub>F-FeOOH)

PAN<sub>A</sub>F-FeOOH was synthesized mainly through a two-step process, as shown in Figure 1.

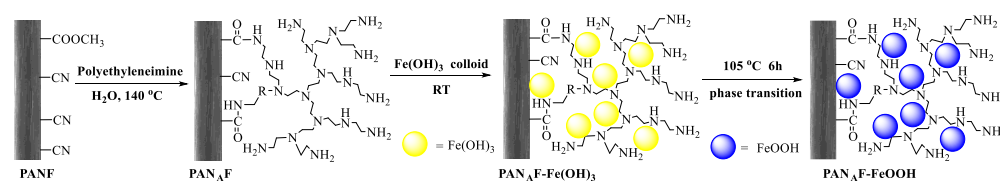


**Figure 1.** The preparation of FeOOH-loaded polyacrylonitrile fiber.

Step 1: PANF (1.0 g) and PEI (5.0 g) were dissolved in a reaction kettle containing 20 mL of H<sub>2</sub>O and then transferred to a reaction kettle at 140 °C for 6 h. After the reaction, the fiber was removed with tweezers and washed with H<sub>2</sub>O (70–80 °C) several times until the pH was neutral. The washed fiber was dried overnight in an oven at 60 °C to obtain aminated PAN<sub>A</sub>F with a weight gain of about 38% (relative to PANF). In addition, PAN<sub>A</sub>Fs with different weight gains (3.58%, 7.99%, 15.09%, 20.99%, 24.39%, 28.39%, and 33.39%) were prepared by adding the substrate of PEI with different contents (0.5, 1, 1.5, 2, 2.5, 3, and 4 g), respectively.

Step 2: First, Fe(OH)<sub>3</sub> colloid solution was prepared: Fe(NO<sub>3</sub>)<sub>3</sub>·9H<sub>2</sub>O (4.04 g) was dissolved in 10 mL of H<sub>2</sub>O, and then it was dropped into 40 mL of boiling deionized water using a drip funnel and stirred vigorously. After cooling at room temperature (25 °C), Fe(OH)<sub>3</sub> colloid solution was obtained. Then, dried 100 mg PAN<sub>A</sub>F was weighed and added to the colloidal solution of Fe(OH)<sub>3</sub>, and the mixture was stirred for 1 h. Finally, the fiber was filtered and placed in an oven at 105 °C for 6 h to obtain PAN<sub>A</sub>F-FeOOH.

### 2.3. Batch Degradation Test of PPOA

Batch degradation tests were carried out in 100 mL glass bottles at 25 °C. The pH of 50 mL of mixed solution containing 5 mg L<sup>-1</sup> PPOA and 0.5 mmol L<sup>-1</sup> PDS was tuned to the target value with 0.1 mol L<sup>-1</sup> H<sub>2</sub>SO<sub>4</sub> and 0.1 mol L<sup>-1</sup> NaOH. Subsequently, 30 mg of dried PAN<sub>A</sub>F-FeOOH was weighed and placed in the above mixed solution for stirring. After regular sampling of 1 mL of the reaction solution, it was immediately filtered using a

0.22  $\mu\text{m}$  needle filter membrane. To end the reaction, the filtrate was immediately mixed with 1 mL of methanol for quenching, and the concentration of the remaining PPOA was tested using high-performance liquid chromatography (HPLC, 1260 Infinity II, Agilent, CA, USA). Meanwhile, various parameters, including initial pH (3–9) and coexisting anions ( $\text{Cl}^-$ ,  $\text{SO}_4^{2-}$ ,  $\text{HCO}_3^-$ , and  $\text{CO}_3^{2-}$ ), influencing PPOA degradation were discussed. In addition, the stability and usefulness of  $\text{PAN}_A\text{F-FeOOH}$  were evaluated through five cycles.

#### 2.4. Phosphate Adsorption on $\text{PAN}_A\text{F-FeOOH}$

Phosphate adsorption experiments used 20 mL glass bottles. The pH of  $\text{KH}_2\text{PO}_4$  (20 mg P  $\text{L}^{-1}$ ) solution was tuned to the target value with 0.1 mol  $\text{L}^{-1}$   $\text{H}_2\text{SO}_4$  and 0.1 mol  $\text{L}^{-1}$  NaOH. Then, 10 mg of dried  $\text{PAN}_A\text{F-FeOOH}$  was weighed and stirred in the above solution (10 mL) until the adsorption equilibrium was obtained, and the remnant phosphate concentration was tested using a visible spectrophotometer (722G, INESA, Shanghai, China). Various influencing parameters, including initial pH value (3–9), different times (0–120 min), different temperatures, different phosphate concentrations (0–50 mg P  $\text{L}^{-1}$ ) and coexisting anions, were also studied. Finally, the stability and practical applicability of  $\text{PAN}_A\text{F-FeOOH}$  for phosphate removal were evaluated by continuous flow experiments and cyclic experiments.

#### 2.5. Analysis and Calculation Methods

The PPOA concentration was determined by HPLC and the phosphate concentration was determined by molybdenum blue spectrophotometry. Detailed procedures and HPLC conditions are described in Section S3 of the supporting information. The % degradation,  $D$  (%), of PPOA by  $\text{PAN}_A\text{F-FeOOH}$  was calculated according to Equation (1):

$$D = \frac{(C_1 - C_2)}{C_1} \times 100\% \quad (1)$$

where  $C_1$  and  $C_2$  are the initial concentration of PPOA and the residual concentration of PPOA after degradation, respectively.

The equilibrium adsorption capacity ( $q_e$ , mg P  $\text{g}^{-1}$ ), adsorption capacity within a certain time ( $q_t$ , mg P  $\text{g}^{-1}$ ), and removal efficiency  $R$  (%) of  $\text{PAN}_A\text{F-FeOOH}$  for phosphate were calculated using the following equations:

$$q_e = \frac{(C_0 - C_e) \times V}{m} \quad (2)$$

$$q_t = \frac{(C_0 - C_t) \times V}{m} \quad (3)$$

$$R = \frac{(C_0 - C_e)}{C_0} \times 100\% \quad (4)$$

where  $C_0$ ,  $C_e$ , and  $C_t$  (mg P  $\text{L}^{-1}$ ) represent the initial concentration of phosphate, the equilibrium concentration of phosphate, and the phosphate concentration at a certain time, respectively.  $V$  (mL) is the solution volume and  $m$  (g) is the fiber mass.

### 3. Results and Discussion

#### 3.1. Synthesis of $\text{PAN}_A\text{F-FeOOH}$

As revealed in Figure 1, the synthesis of aminated polyacrylonitrile fiber ( $\text{PAN}_A\text{F}$ ) was based on our previous research [35]. Amines have strong hydrophilicity and are good metal ligands, so the grafting of PEI on PANF is conducive to the subsequent modification of iron oxides. The modification extent of  $\text{PAN}_A\text{F}$  was calculated by the weight gain.  $\text{PAN}_A\text{F}$  modified to different extents was prepared by regulating the substrate concentration. Then,  $\text{PAN}_A\text{F-FeOOH}$  was constructed using the sol-gel method [38]. Compared with PANF, the

quality of the aminated fiber was significantly increased (3.58–38%), indicating that the amine functional component was successfully loaded on the surface of PANF.

To investigate the effect of the amination degree of PAN<sub>A</sub>F on the synthesis of PAN<sub>A</sub>F-FeOOH, the PPOA removal ability and purification of phosphate by PAN<sub>A</sub>F-FeOOH synthesized from PAN<sub>A</sub>F with different modification degrees were tested (Figure S1). It was found that with increasing weight gain of PAN<sub>A</sub>F, the degradation efficiency of PAN<sub>A</sub>F-FeOOH for PPOA gradually increased; when the weight gain of PAN<sub>A</sub>F was more than 20%, the degradation efficiency was weakly increased (Figure S1a). In terms of phosphate removal, with increasing PAN<sub>A</sub>F weight, the removal capacity for phosphate by the prepared PAN<sub>A</sub>F-FeOOH gradually increased, and the best weight gain of PAN<sub>A</sub>F was about 38% (Figure S1c). The above results showed that more PEI modification was conducive to the fixation of FeOOH on the fiber support, which improved the catalytic or adsorption capacity. Therefore, the optimal weight gain of PAN<sub>A</sub>F was selected as 38%.

Furthermore, the PPOA degradation ability of PAN<sub>A</sub>F-FeOOH prepared with different concentrations of Fe(OH)<sub>3</sub> colloid is demonstrated in Figure S1b. At a concentration of Fe(OH)<sub>3</sub> of 0.3 mol L<sup>-1</sup>, the degradation efficiency reached 90%, while the degradation efficiency decreased with the further increase in the concentration of Fe(OH)<sub>3</sub> colloid. Figure S1d also shows the phosphate adsorption capacity of PAN<sub>A</sub>F-FeOOH prepared with different concentrations of Fe(OH)<sub>3</sub> colloid. Similar to organophosphorus degradation, the trend of phosphate removal by the fiber first increased and then decreased, with the maximum removal ability reached when the concentration of Fe(OH)<sub>3</sub> colloid was 0.2 mol L<sup>-1</sup>. The above results indicated that the supporting of FeOOH was instrumental in improving the catalytic and adsorption capacities of the functionalized fiber. However, when the modification degree of FeOOH was too high, the application effect of PAN<sub>A</sub>F-FeOOH decreased. The reason was that the increased FeOOH modification on the surface of PAN<sub>A</sub>F within a certain range was conducive to increasing the number of effective active sites, but excessive FeOOH modification made it easier to form larger metal oxide particles [38], thus reducing the contact area between the active site and the substrate and thereby reducing its catalytic or adsorption ability. Hence, concentrations of 0.3 and 0.2 mol L<sup>-1</sup> Fe(OH)<sub>3</sub> colloid were selected to synthesize PAN<sub>A</sub>F-FeOOH for organophosphorus degradation and phosphate adsorption, respectively.

### 3.2. Characterization of PAN<sub>A</sub>F-FeOOH

SEM was used to characterize the surface appearance of the functionalized fiber, and the results are presented in Figure 2. Under low magnification (200 times), all of the samples were continuous and showed a complete fiber shape, indicating that the integrity of the fiber was well maintained and had not been damaged (Figure 2, trace a–f). In the SEM images under 2000 times magnification, the surface morphology of PANF was completely flat, and the diameters of PAN<sub>A</sub>F and PAN<sub>A</sub>F-FeOOH were significantly increased due to swelling in the chemical grafting reaction [35]. When the SEM images were enlarged 20,000 times, several fissures appeared on the fiber that increased the contact area between the fiber and the substrate, which was more conducive to catalysis and adsorption [33]. In addition, in the process of PAN<sub>A</sub>F-FeOOH synthesis, an even distribution of iron oxides could be seen on the surface of the fiber when the colloidal concentration of Fe(OH)<sub>3</sub> was lower than 0.3 mol L<sup>-1</sup>; however, when the concentration of Fe(OH)<sub>3</sub> colloid was adjusted to 0.5 mol L<sup>-1</sup>, the iron oxide particles became larger and the uniformity was reduced.

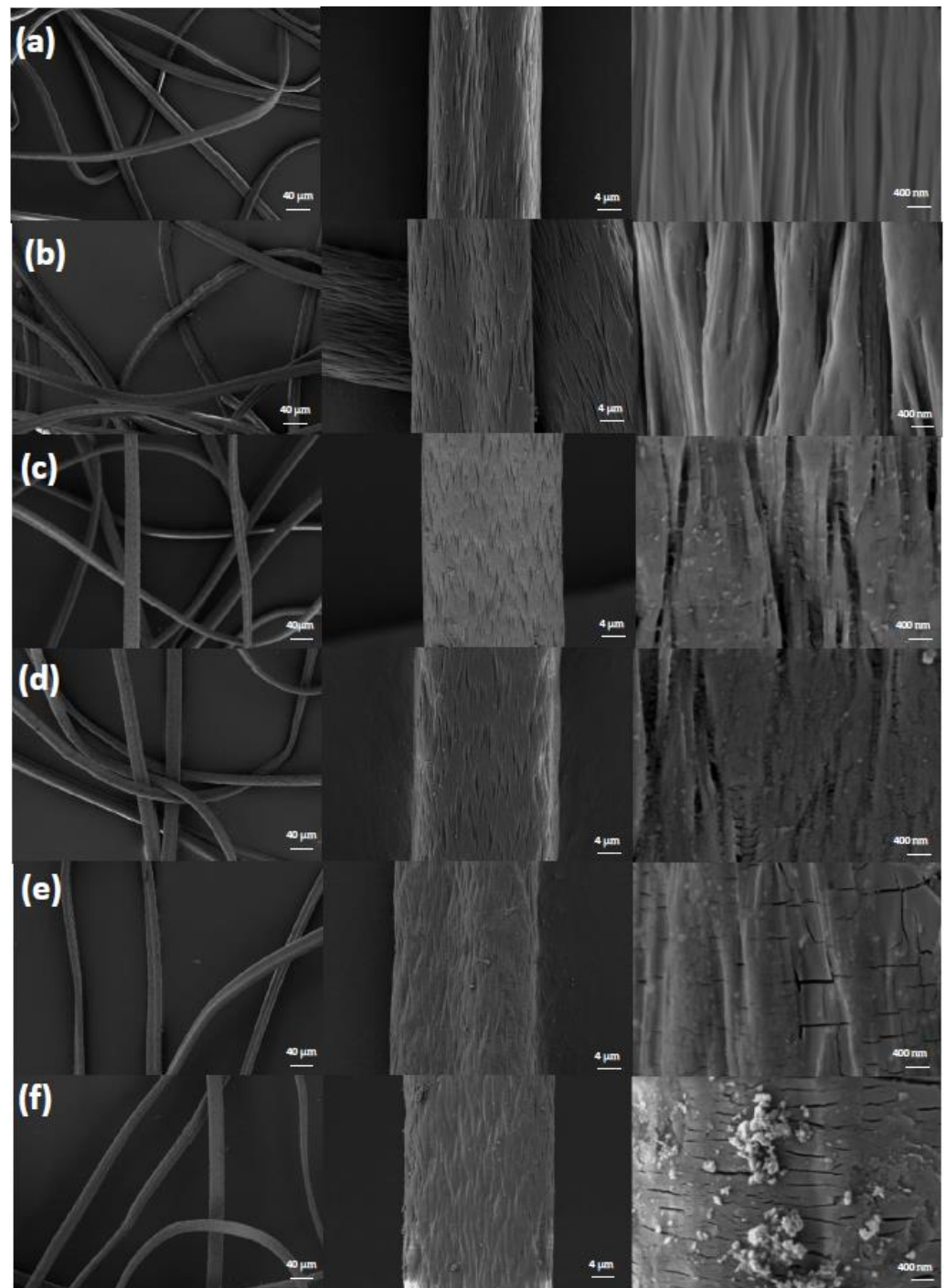


**Figure 2.** The SEM photographs of (a) PANF, (b) PAN<sub>A</sub>F, and (c–f) PAN<sub>A</sub>F-FeOOH prepared with Fe(OH)<sub>3</sub> colloid at 0.05, 0.2, 0.3, and 0.5 mol L<sup>-1</sup>, respectively. Magnifications are 200, 2000, and 20,000 times.

To further demonstrate the successful synthesis of PAN<sub>A</sub>F-FeOOH, energy dispersive spectroscopy (EDS), Fourier-transform infrared spectroscopy (FTIR), X-ray diffraction (XRD), and thermogravimetric analysis (TG) were used, as shown in Figure 3. It was found that compared with PANF and PAN<sub>A</sub>F (Figure 3A, trace a,b), a new characteristic peak of the Fe element appeared in PAN<sub>A</sub>F-FeOOH (Figure 3A, trace c) and the peak intensity of the O element increased, indicating that iron was primarily present in the form of hydroxide on the fiber surface [29]. Changes in the functional groups on the surface of the functionalized fiber were characterized by FTIR. In the spectrum of PANF (Figure 3B,

trace a), the absorption peaks at  $2242\text{ cm}^{-1}$  and  $1732\text{ cm}^{-1}$  could be attributed to the stretching vibration of  $\text{C}\equiv\text{N}$  of the first monomer acrylonitrile and  $\text{C}=\text{O}$  of the second monomer methyl acrylate [39]. Meanwhile,  $\text{PAN}_A\text{F}$  showed a new stretching vibration peak at  $1636\text{ cm}^{-1}$  (Figure 3B, trace b), which was caused by the formation of the amide bond and the  $\text{C}=\text{O}$  tensile vibration [40], indicating that PEI had been successfully loaded onto PANF. Furthermore, the FTIR spectrum of  $\text{PAN}_A\text{F-FeOOH}$  (Figure 3B, trace c) presented a new stretching vibration peak  $671\text{ cm}^{-1}$ , which was caused by the stretching vibration of  $\text{Fe-OH}$  [29], indicating that  $\text{FeOOH}$  had been successfully introduced into the fiber surface. In addition, the characteristic peak of  $1383\text{ cm}^{-1}$  belonged to  $\text{NO}_3^-$  sourced from the starting  $\text{Fe}(\text{NO}_3)_3$  [41], showing that some  $\text{NO}_3^-$  was adsorbed on the fiber surface during the formation of  $\text{FeOOH}$ . The internal crystal structure of the fiber was analyzed by XRD (Figure 3C). The two wide diffraction peaks concentrated at  $17^\circ$  and  $29.5^\circ$  corresponded to the (100) and (110) crystal planes of the hexagonal lattice in PANF [42] (Figure 3C, trace a).  $\text{PAN}_A\text{F}$  and  $\text{PAN}_A\text{F-FeOOH}$  (Figure 3C, traces b,c) had similar characteristic peaks as PANF, showing that the structure of the fiber was not destroyed after functionalization. What's more, new diffraction peaks of  $\text{PAN}_A\text{F-FeOOH}$  were formed at  $2\theta = 55^\circ, 65^\circ,$  and  $75^\circ$ , respectively, which were similar to the characteristic peaks of  $\text{FeOOH}$  reported in the literature [43], further proving that  $\text{FeOOH}$  was truly loaded onto the fiber surface. The thermal stability of the fiber was reflected by TG (Figure 3D). PANF had no obvious quality loss up to  $300^\circ\text{C}$  and still had 9.4% weight remaining at  $800^\circ\text{C}$  (Figure 3D, trace a). After modification, the weight losses of  $\text{PAN}_A\text{F}$  and  $\text{PAN}_A\text{F-FeOOH}$  before  $100^\circ\text{C}$  were mainly caused by water loss because the modified amino group had strong hydrophilicity [35]. The final residual weight of  $\text{PAN}_A\text{F-FeOOH}$  was 41.92%, which was significantly higher than that of PANF and  $\text{PAN}_A\text{F}$ , further illustrating the successful modification of  $\text{FeOOH}$ . The results showed that  $\text{PAN}_A\text{F-FeOOH}$  had good thermal stability and could adapt to an aqueous environment at various temperatures.

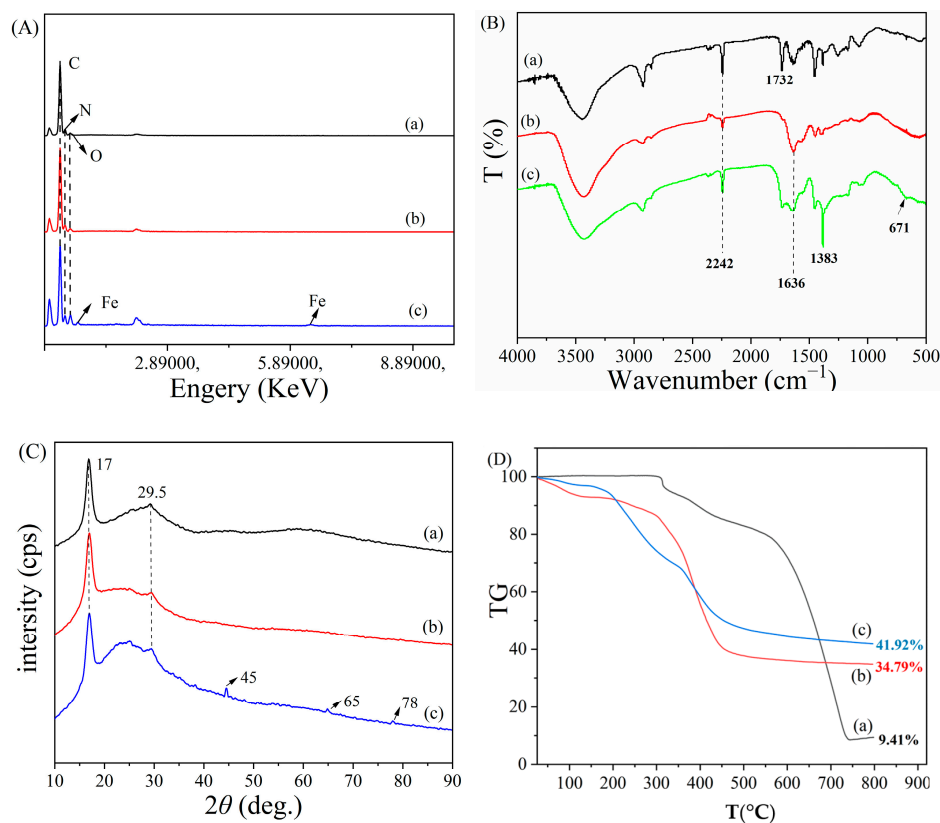


**Figure 3.** (A) The EDS spectra of (a) PANF, (b)  $\text{PAN}_A\text{F}$ , and (c)  $\text{PAN}_A\text{F-FeOOH}$ ; (B) The FTIR spectra of (a) PANF, (b)  $\text{PAN}_A\text{F}$ , and (c)  $\text{PAN}_A\text{F-FeOOH}$ ; (C) The XRD patterns and (D) TGA spectra of (a) PANF, (b)  $\text{PAN}_A\text{F}$ , and (c)  $\text{PAN}_A\text{F-FeOOH}$ .

### Elemental Analysis (EA)

The EA results of the fiber before and after modification are displayed in Table 1. Compared with PANF, the C and N contents of PAN<sub>A</sub>F were significantly decreased and the H content was increased. This was because the molecular formula of PEI is (C<sub>2</sub>H<sub>5</sub>N)<sub>n</sub>; the proportion of C content in PEI (55.81%) was lower than that in PANF (66.17%), while the proportion of H content in PEI (11.63%) was higher than that in PANF (5.179%). The reason for the decrease in N content was that the amination process reduced the N content by converting the cyano groups in PANF to amides through hydrolysis, producing ammonia [44]. Furthermore, PAN<sub>A</sub>F-FeOOH had lower C, N, and H contents than PAN<sub>A</sub>F. The reason was that Fe and O elements were introduced into the PAN<sub>A</sub>F surface, which led to a decrease in the proportion of other elements.

**Table 1.** Elemental analysis data for PANF, PAN<sub>A</sub>F, and PAN<sub>A</sub>F-FeOOH.

Entry	Sample	C (%)	N (%)	H (%)
1	PANF	66.37	24.86	5.18
2	PAN <sub>A</sub> F	55.14	20.15	6.57
3	PAN <sub>A</sub> F-FeOOH	47.32	18.33	4.59

### 3.3. Batch Experiment of PPOA Degradation by PAN<sub>A</sub>F-FeOOH

#### 3.3.1. Conditional Optimization of PPOA Degradation Promoted by PAN<sub>A</sub>F-FeOOH

The effects of pH, PAN<sub>A</sub>F-FeOOH dosage, PDS concentration, and reaction time on the removal of PPOA were studied (Figure 4). It was found that the pH increased from 3 to 5 and the % removal reached 90.2%. With further increase in pH (>5), the % degradation of PPOA significantly decreased to 40.9% at pH of 9 (Figure 4A). This was because the negative charge on the surface of PAN<sub>A</sub>F-FeOOH gradually increased with increasing pH, which increased repulsion with the PDS/PPOA anion, affecting the production of SO<sub>4</sub>•<sup>-</sup> radicals [17]. Furthermore, PAN<sub>A</sub>F-FeOOH dosage also improved the removal of PPOA. The % removal without the addition of PAN<sub>A</sub>F-FeOOH was only 40.2%, while PPOA was nearly completely removed by increasing the mass of PAN<sub>A</sub>F-FeOOH to 30 mg (Figure 4B). The concentration of PDS in the system showed that increasing the concentration of PDS had a positive effect on the removal of PPOA. This was because the increased PDS concentration increased the SO<sub>4</sub>•<sup>-</sup> concentration, which strengthened the degradation effect, and the removal effect was optimal at a concentration of 0.5 mM. However, when the PDS concentration exceeded 0.5 mM, the % removal of PPOA decreased (Figure 4C), probably due to the quenching of SO<sub>4</sub>•<sup>-</sup> with the high concentration of PDS, which caused a decrease in the % degradation of PPOA [45]. Compared with cobalt–yttrium binary oxide [11], PAN<sub>A</sub>F-FeOOH degraded PPOA with lower persulfate concentration. The effect of reaction time on the removal of PPOA at various temperatures was also explored (Figure 4D). The removal efficiency of PPOA gradually increased within 120 min, which could reach more than 90%. In addition, increasing temperature was conducive to the degradation reaction. This was because increasing temperature was beneficial to accelerating the reaction rate of catalytic PDS, thus increasing the generation of SO<sub>4</sub>•<sup>-</sup> and improving the degradation efficiency of PPOA [46]. It is worth mentioning that the degradation of PPOA could be efficiently carried out at room temperature, showing high practical application value.

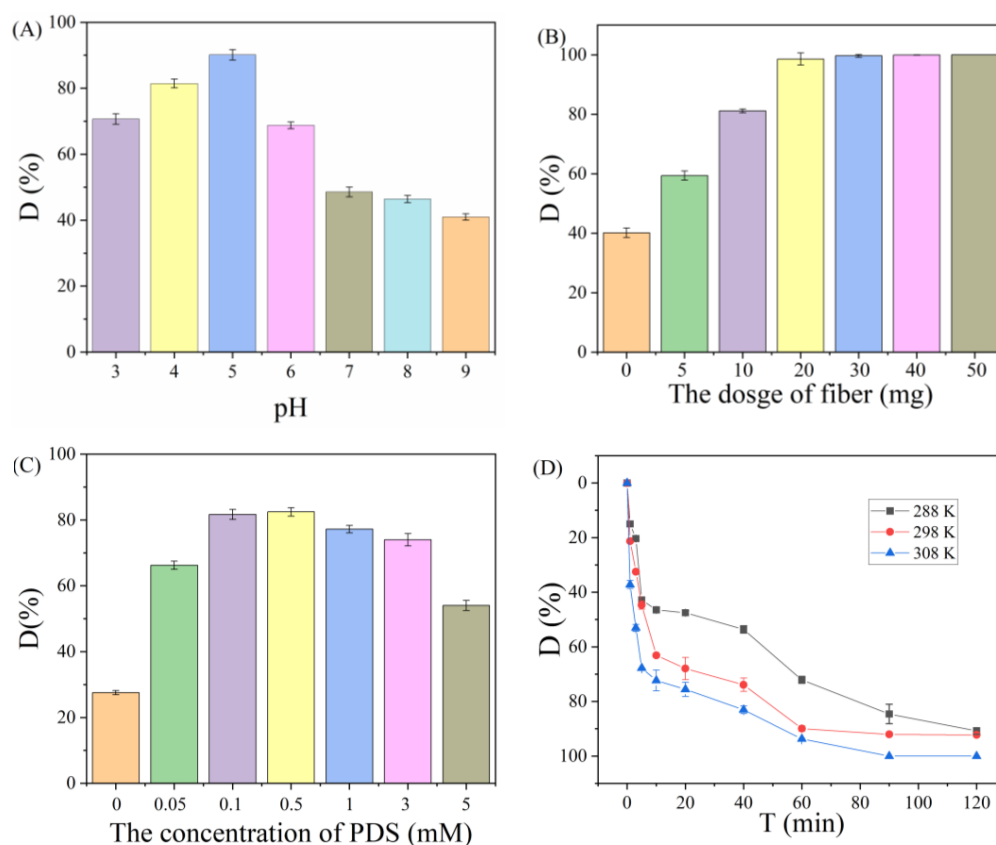


**Figure 4.** Influence of (A) pH, (B) fiber dosage, (C) PDS concentration, and (D) reaction time on PPOA degradation.

### 3.3.2. Influence of Coexisting Ions and Reusability of PAN<sub>A</sub>F-FeOOH

The presence of coexisting anions in the aqueous environment becomes one of the important interfering factors in the activation of PDS [47]. As shown in Figure 5A, the effect of different coexisting ions on the degradation ability was investigated. While the introduction of  $\text{Cl}^-$  resulted in only 33.62% degradation of PPOA, this phenomenon was chiefly due to the simultaneous production of less active  $\text{Cl}\bullet$ ,  $\text{Cl}_2\bullet^-$ , and  $\text{HOCl}$  products initiated by  $\text{SO}_4\bullet^-$  in the reaction process [48], which reduced the % degradation of PPOA. Positively, the coexisting anions of  $\text{CO}_3^{2-}$ ,  $\text{SO}_4^{2-}$ , and  $\text{HCO}_3^-$  did not significantly affect the degradation process. Compared with  $\text{Co}_3\text{O}_4\text{-La}_2\text{O}_2\text{CO}_3/\text{C}$ -derived MOF materials [17], PAN<sub>A</sub>F-FeOOH was better adapted to complex ionic environments, indicating that PAN<sub>A</sub>F-FeOOH had potential application value in actual water bodies. In addition, the recyclability of PAN<sub>A</sub>F-FeOOH was explored (Figure 5B). The % removal of PPOA could reach 99% in the first three cycles, while the % removal in the fifth cycle was 78.23%, which may have been caused by the partial deactivation of the loaded catalyst and the loss of FeOOH during the degradation process [23]. The good reusability showed that PAN<sub>A</sub>F-FeOOH had good stability and practicability.

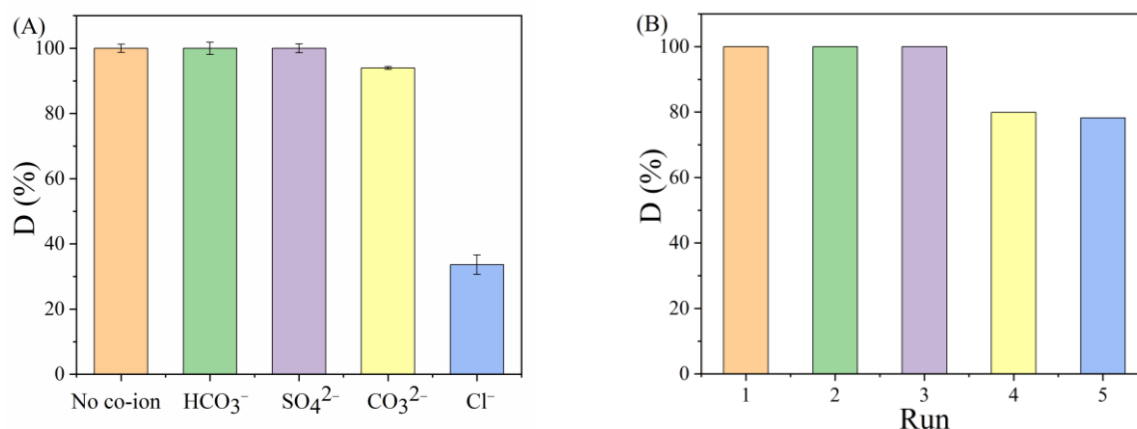


**Figure 5.** (A) The impact of coexisting ions on PPOA degradation; (B) renewability of PAN<sub>A</sub>F-FeOOH for PPOA degradation.

### 3.4. Batch Experiment of Phosphate Adsorption by PAN<sub>A</sub>F-FeOOH

#### 3.4.1. Influence of pH

In actual wastewater, due to its complex composition, the applicable pH range of the adsorbent is an important aspect. Therefore, the adsorption capacity of PAN<sub>A</sub>F-FeOOH for phosphate was measured under initial pH 3–9. As shown in Figure 6A, it was found that the phosphate removal by PAN<sub>A</sub>F-FeOOH increased rapidly with increasing pH value from 3 to 7, and reached the maximum value when pH = 7. Under alkaline conditions (pH 8–9), the adsorption capacity for phosphate by PAN<sub>A</sub>F-FeOOH slightly decreased. These results were similar to those of other Fe-based materials previously reported in the literature [49]. Additionally, this phenomenon may have been related to the dissociation equilibrium of phosphate. According to the relationship between the distribution of phosphate species and pH value, when pH = 2–3, phosphates mostly exist in the form of H<sub>3</sub>PO<sub>4</sub>, which could not be effectively adsorbed on the surface of PAN<sub>A</sub>F-FeOOH through electrostatic interaction and would result in a relatively low phosphate adsorption capacity. When the pH is 3–7, H<sub>2</sub>PO<sub>4</sub><sup>-</sup> and HPO<sub>4</sub><sup>2-</sup> are the main forms of phosphate, and these forms of phosphate were easily adsorbed by the iron site leached from the PAN<sub>A</sub>F-FeOOH surface. There were two main reasons for the decreased phosphate adsorption at pH 8–9. First, under alkaline conditions, PAN<sub>A</sub>F-FeOOH had too much negative charge on the surface, which led to the enhancement of electrostatic repulsion. Secondly, P and hydroxide ion (OH<sup>-</sup>) competed for adsorption sites on the PAN<sub>A</sub>F-FeOOH surface, resulting in a decrease in phosphate adsorption capacity [50].

#### 3.4.2. Influence of Coexisting Ions

Due to the existence of various anions (Cl<sup>-</sup>, NO<sub>3</sub><sup>-</sup>, CO<sub>3</sub><sup>2-</sup>, and SO<sub>4</sub><sup>2-</sup>) in wastewater, the removal ability of PAN<sub>A</sub>F-FeOOH for phosphate may be affected. In order to verify the selectivity of PAN<sub>A</sub>F-FeOOH for phosphate adsorption, the purification of phosphate by PAN<sub>A</sub>F-FeOOH in the presence of coexisting ions was determined. As depicted in Figure 6B, the existence of Cl<sup>-</sup>, NO<sub>3</sub><sup>-</sup>, and CO<sub>3</sub><sup>2-</sup> had little influence on phosphate adsorption by the fiber, while the presence of SO<sub>4</sub><sup>2-</sup> could significantly inhibit phosphate adsorption. The reason may have been the strong affinity between SO<sub>4</sub><sup>2-</sup> and Fe on the surface of PAN<sub>A</sub>F-FeOOH, which would compete with phosphate for its adsorption site, thus inhibiting phosphate adsorption [50]. Despite these findings, PAN<sub>A</sub>F-FeOOH still had a certain adsorption capacity for phosphate in the presence of SO<sub>4</sub><sup>2-</sup>. This indicated that PAN<sub>A</sub>F-FeOOH could efficiently remove phosphate in actual water with multiple anions, showing strong practical application capability.

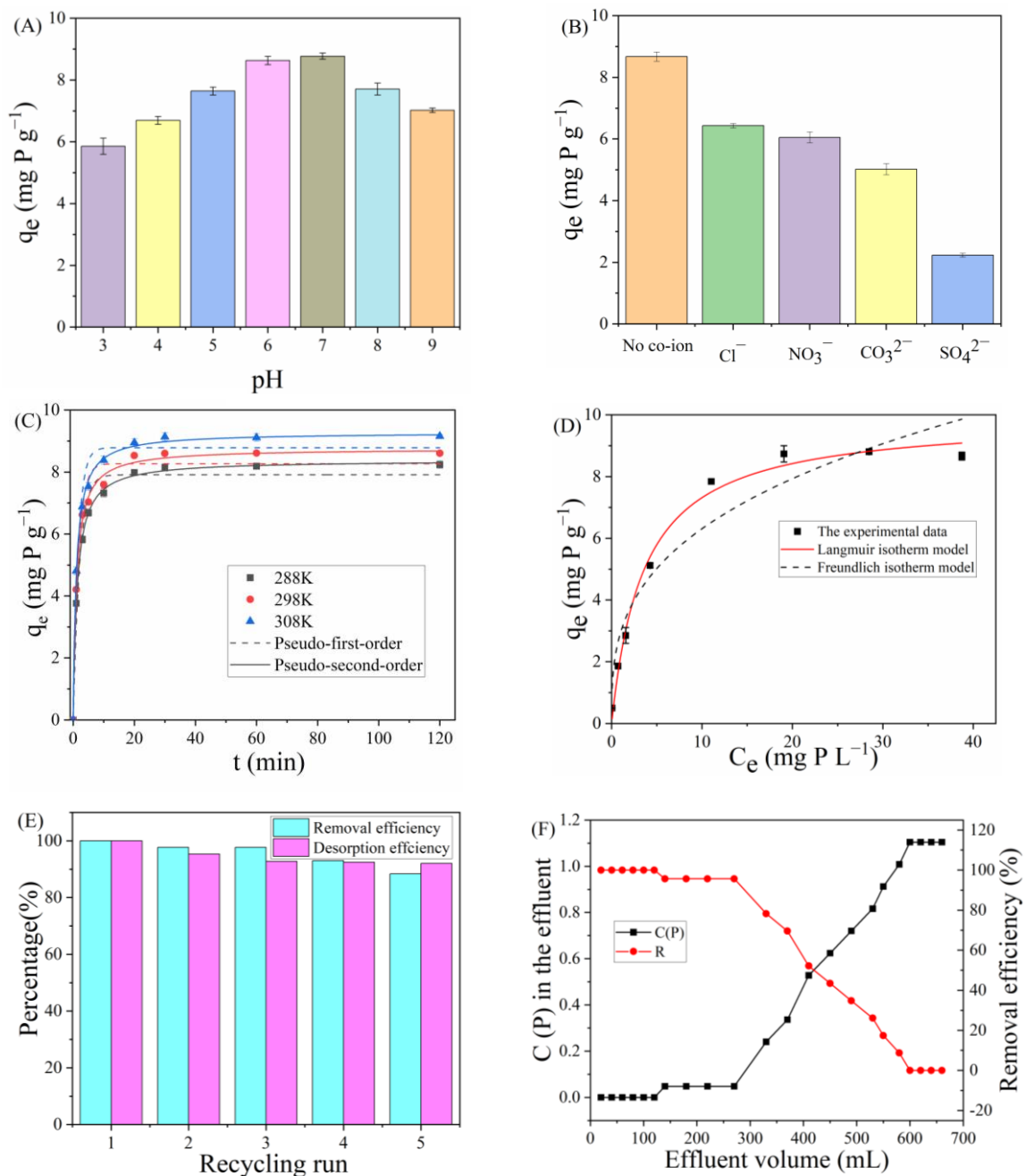


**Figure 6.** The influence of (A) pH, (B) coexisting anions, (C) contact time, and (D) initial phosphate concentration on phosphate removal by PAN<sub>A</sub>F-FeOOH. (E) Reusability of PAN<sub>A</sub>F-FeOOH for phosphate removal and (F) breakthrough curves of phosphate solutions in continuous flow conditions.

### 3.4.3. Adsorption Kinetics and Thermodynamics

The study of adsorption kinetics is a key method used to study the reaction path of adsorbents. As revealed in Figure 6C, the time-dependent adsorption capacity of PAN<sub>A</sub>F-FeOOH for phosphate at 288, 298, and 308 K was studied. The trend of the three curves was roughly the same, with fast adsorption occurring in the first 20 min, followed by a slow adsorption rate, and reaching adsorption equilibrium after 30 min. The result demonstrated that at the beginning, the bulk of the active sites exposed on the fiber surface could quickly capture phosphate in water. With the passage of time, the adsorption process slowed down after the surface adsorption active sites of the adsorbent gradually reached saturation.

In order to better explore the adsorption mechanism of phosphate on PAN<sub>A</sub>F-FeOOH, the data were fitted by pseudo first-order kinetics (5) and pseudo second-order kinetics (6), respectively. The formulas of the different dynamics are as follows:

$$q_e = (1 - e^{-K_1 t}) \quad (5)$$

$$q_e = \left( \frac{K_2 q_e^2 t}{1 + K_2 q_e t} \right) \quad (6)$$

where  $K_1$  and  $K_2$  are the pseudo first-order and pseudo second-order kinetics adsorption rate constants, respectively. The fitted figure and kinetic parameters are presented in Figure 6C and Table S1, respectively. The  $R^2$  values of the second-order kinetic model were all higher than those of the first-order kinetic model (Table S1), and the  $q_e$  fitted by the pseudo second-order kinetics model was closer to the actual  $q_e$ . The results illustrated that the adsorption process of phosphate by PAN<sub>A</sub>F-FeOOH was more inclined to the pseudo second-order kinetics model, showing a chemical adsorption process.

High temperatures promote inter-molecular movement and thus have a certain influence on the adsorption process, as shown in Figure 6C. It was found that the removal ability of PAN<sub>A</sub>F-FeOOH for phosphate increased with rising temperature, which showed that the adsorption process was an endothermic reaction. Furthermore, the thermodynamic parameters of  $\Delta S^0$  (standard entropy,  $\text{J mol}^{-1} \text{K}^{-1}$ ),  $\Delta H^0$  (standard enthalpy,  $\text{kJ mol}^{-1}$ ), and  $\Delta G^0$  (Gibbs free energy,  $\text{kJ mol}^{-1}$ ) were further used to reveal the relationship between temperature and phosphate adsorption, which were calculated using the following equations:

$$K_c = \frac{q_e}{C_e} \quad (7)$$

$$\Delta G^0 = -RT \ln K_c \quad (8)$$

$$\ln K_c = \frac{\Delta S^0}{R} - \frac{\Delta H^0}{RT} \quad (9)$$

where  $K_c$  was the distribution coefficient,  $R$  was the gas constant ( $8.314 \text{ J mol}^{-1} \text{ k}^{-1}$ ), and  $T$  was the temperature (K), respectively. The  $\Delta S^0$  and  $\Delta H^0$  could be calculated by plotting  $\ln K_c$  versus  $1/T$ , and the relevant curves and calculated parameters are displayed in Figure S2 and Table S2, respectively. The  $\Delta G^0$  was negative, showing that the removal of phosphate by PAN<sub>A</sub>F-FeOOH adsorbent was spontaneous. Furthermore, the absolute value of  $\Delta G^0$  increased with rising temperature, which meant that the higher the temperature, the more natural the reaction.  $\Delta H^0$  values were positive, suggesting that phosphate adsorption by PAN<sub>A</sub>F-FeOOH is an endothermic reaction. In addition, a positive  $\Delta S^0$  value meant that the randomness of the solid/solution interface increased irregularly during phosphate adsorption.

#### 3.4.4. Adsorption Isotherm

In order to reveal the adsorption capacity of PAN<sub>A</sub>F-FeOOH for phosphate, isothermal adsorption experiments were carried out at room temperature with different initial phosphate concentrations. As shown in Figure 6D, the adsorption ability of PAN<sub>A</sub>F-FeOOH for phosphate increased with the initial concentration of phosphate until the adsorption saturation was reached. This may have been due to the presence of more coordination sites for phosphorus at lower concentrations, and the active adsorption sites became saturated with increasing phosphorus concentrations. Moreover, Langmuir (10) and Freundlich (11) adsorption isotherm models were used to fit the adsorption data, the equations of which are as follows:

$$q_e = \frac{K_L q_m C_e}{1 + K_L C_e} \quad (10)$$

$$q_e = K_F C_e^{1/n} \quad (11)$$

where  $q_m$  is the theoretical maximum adsorption estimated by the Langmuir model,  $K_L$  is the Langmuir constant, and  $K_F$  and  $n$  are the Freundlich constant and homogeneity coefficient, respectively. The graphs and related data obtained by fitting curves are located in Figure 6D and Table S3, respectively.

The result showed that the  $R^2$  values of the fitting curve of the Langmuir model were larger than those of the Freundlich model (Table S3), which indicated that the Langmuir model was more suitable for the adsorption of phosphate by PAN<sub>A</sub>F-FeOOH. Therefore, the adsorption of phosphate by the fiber tended to be uniform monolayer adsorption. It is worth mentioning that the maximal adsorption amount calculated by Langmuir was 9.92 mg P g<sup>-1</sup>, which was higher than that reported in other literature for iron-modified composite phosphorus adsorbents such as solid carbon source/zero-valent iron composite (0.21 mg P g<sup>-1</sup>) [51], Fe-modified corn straw biochar (0.56 mg P g<sup>-1</sup>) [52], and iron-containing activated carbon (8.47 mg P g<sup>-1</sup>). Hence, PAN<sub>A</sub>F-FeOOH showed great potential for phosphate removal from water.

#### 3.4.5. Reusability and Continuous Flow Application of PAN<sub>A</sub>F-FeOOH

To explore the regeneration capacity of PAN<sub>A</sub>F-FeOOH as a phosphate removal adsorbent, PAN<sub>A</sub>F-FeOOH saturated with phosphate was eluted with 0.05 mol L<sup>-1</sup> NaOH for 1 h. As shown in Figure 6E, the % phosphate removal by PAN<sub>A</sub>F-FeOOH tenuously decreased after 5 cycles, and the fiber still maintained a % phosphate removal of more than 88%. This result demonstrated that PAN<sub>A</sub>F-FeOOH had excellent stability and reusability.

Furthermore, a continuous flow experiment was carried out to verify the practical application capability of PAN<sub>A</sub>F-FeOOH. The continuous flow device is shown in Figure S3. Dried PAN<sub>A</sub>F-FeOOH (300 mg) was placed in a silicone tube (length 100 mm, diameter 5.6 mm), Chaohu Lake water with an initial concentration of 1 mg P L<sup>-1</sup> was injected at a flow rate of 1 mL min<sup>-1</sup> using a peristaltic pump (the concentration of Chaohu Lake water was specially adjusted to 1 mg P L<sup>-1</sup>), and then the concentration of phosphate in the receiving solution was determined. The penetration curves of PAN<sub>A</sub>F-FeOOH for phosphate removal were plotted (Figure 6F), and it was found that with increasing phosphate outflow liquid volume, its concentration gradually increased. When the volume of liquid was less than 280 mL, the % phosphate removal could be maintained above 95%. This result suggested that PAN<sub>A</sub>F-FeOOH could effectively purify phosphate under continuous flow conditions. Repeating the fiber multiple times could be used as an important building material to enhance the mechanical strength of cement [53].

#### 3.5. Mechanisms of PPOA Degradation and Phosphate Adsorption by PAN<sub>A</sub>F-FeOOH

In this work, reactive oxygen species (ROS) were determined by electron paramagnetic resonance (EPR) to describe the key free radicals in the PPOA degradation process (Figure S4). The EPR results showed that the signal strength of SO<sub>4</sub>•<sup>-</sup> and •OH catalyzed by PAN<sub>A</sub>F-FeOOH was significantly improved when compared with the pure PDS system. Additionally, the peak intensity of SO<sub>4</sub>•<sup>-</sup> was higher than that of •OH (Figure S4A), while the strength of singlet oxygen <sup>1</sup>O<sub>2</sub> had no obvious change (Figure S4B). The above phenomena explained that SO<sub>4</sub>•<sup>-</sup> and •OH were the two dominant active species for PPOA degradation. The reason was that SO<sub>4</sub>•<sup>-</sup> could be slowly generated by dissociation of the peroxide bond [54], and Fe<sup>3+</sup> on the fiber catalyst could react with S<sub>2</sub>O<sub>8</sub><sup>2-</sup> to produce Fe<sup>2+</sup> and the persulfate radical (S<sub>2</sub>O<sub>8</sub>•) [25]. The newly produced Fe<sup>2+</sup> could activate persulfate to produce the sulfate radical [55], hence Fe<sup>2+</sup> was continuously produced through the above electron transfer reaction, which improved the efficiency of SO<sub>4</sub>•<sup>-</sup> generation. In the PPOA degradation system, SO<sub>4</sub>•<sup>-</sup> was preferentially produced, then it reacted with H<sub>2</sub>O to produce •OH. In addition to ROS participating in the degradation of PPOA, the enrichment ability of PAN<sub>A</sub>F-FeOOH for adsorption of PPOA was also an important factor for efficient catalysis. Relevant research shows that improving the affinity and adsorption capacity of

the catalyst for the substrate is conducive to improving its catalytic capacity [56,57]. To verify this assumption, the adsorption capacity of PAN<sub>A</sub>F-FeOOH for PPOA was studied (Figure S5). PANF had little enrichment capacity for PPOA adsorption; however, after amination and FeOOH modification, the % removal of PPOA by the functionalized fiber was obviously increased to 40% and 45%, respectively. Similar to our previous research [31], the above results showed that the functionalized modification of the fiber support created a microenvironment on the surface of the fiber that was conducive to the entry of PPOA, which made it easier to degrade by the ROS generated by the activated persulfate of PAN<sub>A</sub>F-FeOOH. This was because the existence of the microenvironment effect shortened the diffusion distance of reactive oxygen radicals, thus accelerating the degradation of PPOA.

Under optimal degradation conditions, when the degradation reaction was over, the inorganic phosphorus and total phosphorus in the solution were determined by molybdenum blue colorimetry and ICP-OES (ICP-MS, Thermo scientific, Waltham, MA, USA), respectively. The results showed that there was a small amount of phosphate in the solution and the concentration of total phosphorus was about 10% of the original concentration, indicating that PAN<sub>A</sub>F-FeOOH successfully degraded PPOA and simultaneously absorbed the degradation product of inorganic phosphorus. Hence, the phosphate adsorption mechanism of PAN<sub>A</sub>F-FeOOH was further studied by X-ray photoelectron spectroscopy (XPS), as shown in Figure 7, and the atomic percentage of the fiber is presented in Table S4. As depicted in Figure 7A, similar to the results of EDS, a new peak of Fe emerged in the PAN<sub>A</sub>F-FeOOH spectrum, indicating the successful grafting of FeOOH on the fiber (Figure 7A, trace c). After adsorption of phosphate, the high-resolution spectrum of PAN<sub>A</sub>F-FeOOH-P possessed the characteristic peak of P 2p (Figure 7B), which was direct evidence of phosphate adsorption by PAN<sub>A</sub>F-FeOOH.

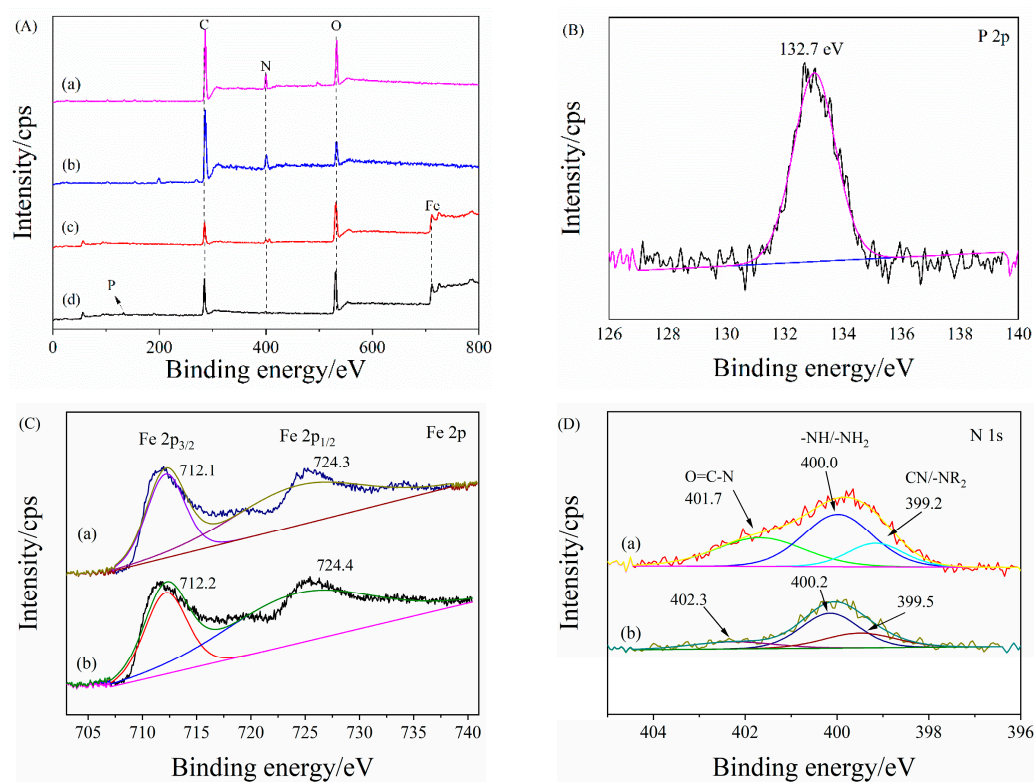


**Figure 7.** (A) XPS survey of (a) PANF, (b) PAN<sub>A</sub>F, (c) PAN<sub>A</sub>F-FeOOH, and (d) PAN<sub>A</sub>F-FeOOH-P; (B) High-resolution spectrum of P 2p for PAN<sub>A</sub>F-FeOOH-P; (C) High-resolution Fe 2p spectrum of (a) PAN<sub>A</sub>F-FeOOH and (b) PAN<sub>A</sub>F-FeOOH-P; (D) High-resolution N 1s spectrum of (a) PAN<sub>A</sub>F-FeOOH and (b) PAN<sub>A</sub>F-FeOOH-P.

The high-resolution spectrum of Fe 2p for PAN<sub>A</sub>F-FeOOH was parsed into 2p<sub>1/2</sub> at 724.4 eV and 2p<sub>3/2</sub> at 712.4 eV (Figure 7C, trace a). The binding energies of Fe 2p for PAN<sub>A</sub>F-FeOOH-P (Figure 7C, trace b) were weakly reduced to 724.3 and 712.1 eV, which was due to the formation of the Fe–O–P bond between phosphate and Fe modified on the fiber, resulting in the increased electron cloud density of the atom [58]. The results indicated that the iron modified on the fiber surface played an significant role in phosphate adsorption. Furthermore, the high-resolution spectrum of N 1s was decomposed into 401.6, 400.0, and 399.2 eV, which were the characteristic peaks of O≡C–N, –NH–/–NH<sub>2</sub>, and –NR<sub>2</sub>, respectively [33]. After adsorption of phosphate, the binding energies of the N1s spectrum slightly increased because the protonated amine group on the fiber surface combined with phosphate through electrostatic force [59]. Hence, the removal mechanism of phosphate by PAN<sub>A</sub>F-FeOOH-P was mainly due to the strong binding force of iron and the electrostatic force of protonated amine.

### 3.6. Comparison of Different FeOOH Phosphate Adsorbents

The comparison of phosphate adsorption by the fiber was performed as follows. In this study, the adsorption capacity, cycling performance, and equilibrium time of PAN<sub>A</sub>F-FeOOH were compared with other adsorbents for phosphate removal (Table S5). PAN<sub>A</sub>F-FeOOH had a better phosphate adsorption capacity than other adsorbents (Table S5, entries 1 and 5), and the cycling performance of the fiber (5 times) was higher than that of other adsorbents. Furthermore, PAN<sub>A</sub>F-FeOOH reached adsorption equilibrium (30 min) faster than the other adsorbent materials. Overall, PAN<sub>A</sub>F-FeOOH showed high phosphate removal efficiency, good adsorption capacity, and excellent reusability.

### 3.7. Practical Application Capability Test of PAN<sub>A</sub>F-FeOOH

This study also tested the practical application capability of PAN<sub>A</sub>F-FeOOH to remove phosphorus in actual water and simulated wastewater, respectively. The total phosphorus concentration was adjusted to about 1 mg P L<sup>-1</sup> (0.5 mg P L<sup>-1</sup> PPOA + 0.5 mg P L<sup>-1</sup> KH<sub>2</sub>PO<sub>4</sub>) in both real water (Chaohu Lake, China) and deionized water. Dried 50 mg of PAN<sub>A</sub>F-FeOOH and 0.5 mmol L<sup>-1</sup> of PDS were added to 20 mL of the above water samples, and the remaining total phosphorus concentration was measured after stirring for 1 h. The total phosphorus concentration in the water samples before and after fiber treatment were measured. The results showed that PAN<sub>A</sub>F-FeOOH could effectively remove 83.6% of total phosphorus in the water sample of Chaohu Lake, while the % removal reached 90.4% in the simulated wastewater. The application capability of the fiber in real water bodies was slightly lower than that in simulated wastewater samples, possibly due to complex coexisting ion interference in real water bodies. Altogether, PAN<sub>A</sub>F-FeOOH showed excellent application ability for phosphorus removal in real water.

## 4. Conclusions

In this work, a novel FeOOH-modified polyacrylonitrile fiber (PAN<sub>A</sub>F-FeOOH) was intelligently synthesized for the simultaneous removal of organophosphorus and phosphate. PAN<sub>A</sub>F with a weight gain of 38% and iron concentrations of 0.2 and 0.3 mol L<sup>-1</sup> were the optimal synthesis conditions for organophosphorus degradation and phosphate adsorption, respectively, by the PAN<sub>A</sub>F-FeOOH. The degradation conditions for phenylphosphonic acid (PPOA) were optimized, and the PAN<sub>A</sub>F-FeOOH (30 mg) was able to activate PDS (0.5 mmol L<sup>-1</sup>) to remove more than 99% of PPOA (0.5 mg L<sup>-1</sup>, pH = 5) within 1.5 h. Positively, phosphate produced by the degradation process could be efficiently adsorbed by the PAN<sub>A</sub>F-FeOOH. Hence, the phosphate adsorption by the PAN<sub>A</sub>F-FeOOH was investigated. The fiber showed wide pH adaptability with a maximum removal capacity of 9.92 mg P g<sup>-1</sup>, which was higher than most reported iron-based functional materials. Furthermore, the PAN<sub>A</sub>F-FeOOH possesses the advantages of anti-interference with coexisting ions, excellent recyclability (5 times), and continuous flow application. In addition, electron paramagnetic resonance and X-ray photoelectron spectroscopy were used to clarify the

promotion mechanism of the fiber surface microenvironment. It was found that  $\text{SO}_4^{\bullet-}$  and  $\bullet\text{OH}$  were the key radicals for PPOA degradation, and the strong enrichment ability of the functional moieties on the fiber surface also accelerated the removal of PPOA. In addition, the phosphate removal mechanism was chiefly attributed to the synergy of Fe and amine groups. This research provides new ideas for the simultaneous removal of organic and inorganic phosphorus, which is of great significance for pollution remediation and the reuse of organic phosphorus.

**Supplementary Materials:** The following supporting information can be downloaded at: <https://www.mdpi.com/article/10.3390/polym15081918/s1>, References [60–65] are cited in supplementary material. Figure S1: (a) The degradation effect of PPOA by 0.3 mol/L  $\text{Fe}(\text{OH})_3$  combined with aminated fibers with different weight gains; (b) The degradation effect of PPOA by aminated fiber with a weight gain of 38% combined with different concentrations of  $\text{Fe}(\text{OH})_3$  colloid; (c) Phosphate adsorption capacity of 0.2 mol/L  $\text{Fe}(\text{OH})_3$  combined with aminated fibers with different weight gains; (d) Phosphate adsorption capacity of aminated fiber with a weight gain of 38% combined with different concentrations of  $\text{Fe}(\text{OH})_3$  colloid. Figure S2: Fitting diagram of thermodynamics of phosphate. Figure S3: Simple diagram of continuous flow process device. Figure S4: (A) EPR spectrum of  $\text{SO}_4^{\bullet-}$  and  $\bullet\text{OH}$  of PDS/PDS- $\text{PAN}_A\text{F-FeOOH}$  catalytic system; (B) EPR spectrum of  $^1\text{O}_2$  of PDS/PDS- $\text{PAN}_A\text{F-FeOOH}$  catalytic system. Figure S5: Adsorption capacity of  $\text{PAN}_A\text{F-FeOOH}$  for PPOA. Table S1: Kinetic parameters of phosphate adsorption by  $\text{PAN}_A\text{F-FeOOH}$ . Table S2: Thermodynamic parameters of phosphate adsorption by  $\text{PAN}_A\text{F-FeOOH}$ . Table S3: Isotherm parameters of phosphate adsorption by  $\text{PAN}_A\text{F-FeOOH}$ . Table S4: The mass and atomic percentage of the functionalized fiber obtained by XPS. Table S5. Comparison of different phosphate adsorbents.

**Author Contributions:** Conceptualization, G.X.; methodology, Q.X. and W.Z.; validation, R.Z. and W.X.; formal analysis, S.Z.; investigation, P.L.; resources, C.Z.; data curation, R.Z. and W.X.; writing—original draft preparation, R.Z. and W.X.; writing—review and editing, G.X.; visualization, W.Z.; supervision, X.Y.; project administration, G.X.; funding acquisition, G.X., C.Z. and Q.X. All authors have read and agreed to the published version of the manuscript.

**Funding:** This work was financially supported by the National Natural Science Foundation of China (Grant No. 22208003), Major Science and Technology Projects in Anhui Province (No. 202103a06020012), and the Opening Foundation of The Technology Center of Anhui Chaoyue Environmental Protection Technology Co., Ltd. (2022-KYJJ-3).

**Institutional Review Board Statement:** Not applicable.

**Data Availability Statement:** The data presented in this work are available upon request from the corresponding author.

**Acknowledgments:** Thank you to Longjin Jiang from The Technology Center of Anhui Chaoyue Environmental Protection Technology Co., Ltd. We sincerely thank him for his financial support and for his valuable comments during the revision and improvement of the paper.

**Conflicts of Interest:** The authors declare no conflict of interest.

## References

1. Zhao, Y.; Guo, L.; Shen, W.; An, Q.; Xiao, Z.; Wang, H.; Cai, W.; Zhai, S.; Li, Z. Function integrated chitosan-based beads with throughout sorption sites and inherent diffusion network for efficient phosphate removal. *Carbohydr. Polym.* **2020**, *230*, 115639. [[CrossRef](#)] [[PubMed](#)]
2. Zong, E.; Huang, G.; Liu, X.; Lei, W.; Jiang, S.; Ma, Z.; Wang, J.; Song, P. A lignin-based nano-adsorbent for superfast and highly selective removal of phosphate. *J. Mater. Chem. A* **2018**, *6*, 9971–9983. [[CrossRef](#)]
3. Zhang, J.; Tang, L.; Tang, W.; Zhong, Y.; Luo, K.; Duan, M.; Xing, W.; Liang, J. Removal and recovery of phosphorus from low-strength wastewaters by flow-electrode capacitive deionization. *Sep. Purif. Technol.* **2020**, *237*, 116322. [[CrossRef](#)]
4. Yang, C.; Li, J.; Yin, H. Phosphorus internal loading and sediment diagenesis in a large eutrophic lake (Lake Chaohu, China). *Environ. Pollut.* **2022**, *292*, 118471. [[CrossRef](#)] [[PubMed](#)]
5. Malone, T.C.; Newton, A. The Globalization of Cultural Eutrophication in the Coastal Ocean: Causes and Consequences. *Front. Mar. Sci.* **2020**, *7*, 670.
6. Ni, Z.K.; Wang, S.R.; Zhang, B.T.; Wang, Y.M.; Li, H. Response of sediment organic phosphorus composition to lake trophic status in China. *Sci. Total Environ.* **2019**, *652*, 495–504. [[CrossRef](#)]

7. Ajiboye, B.; Akinremi, O.O.; Racz, G.J. Laboratory characterization of phosphorus in fresh and oven-dried organic amendments. *J. Environ. Qual.* **2004**, *33*, 1062–1069. [[CrossRef](#)]
8. Dou, Z.; Toth, J.D.; Galligan, D.T.; Ramberg, C.F.; Ferguson, J.D. Laboratory procedures for characterizing manure phosphorus. *J. Environ. Qual.* **2000**, *29*, 508–514. [[CrossRef](#)]
9. Aimer, Y.; Benali, O.; Serrano, K.G. Study of the degradation of an organophosphorus pesticide using electrogenerated hydroxyl radicals or heat-activated persulfate. *Sep. Purif. Technol.* **2019**, *208*, 27–33. [[CrossRef](#)]
10. Rott, E.; Steinmetz, H.; Metzger, J.W. Organophosphonates: A review on environmental relevance, biodegradability and removal in wastewater treatment plants. *Sci. Total Environ.* **2018**, *615*, 1176–1191. [[CrossRef](#)]
11. Chen, C.; Pang, Y.Q.; Li, Y.X.; Li, W.; Lan, Y.Q.; Shen, W.B. Dual functional cobalt-yttrium binary oxide activation of peroxy-monosulfate for degradation of phenylphosphonic acid and simultaneous adsorption of phosphate product. *Chem. Eng. J.* **2022**, *429*, 132185. [[CrossRef](#)]
12. Li, G.; Wang, B.; Xu, W.Q.; Han, Y.; Sun, Q. Rapid TiO<sub>2</sub>/SBA-15 synthesis from ilmenite and use in photocatalytic degradation of dimethoate under simulated solar light. *Dyes Pigment.* **2018**, *155*, 265–275. [[CrossRef](#)]
13. Feng, H.; Mao, W.; Li, Y.; Wang, X.; Chen, S. Characterization of dissolved organic matter during the O<sub>3</sub>-based advanced oxidation of mature landfill leachate with and without biological pre-treatment and operating cost analysis. *Chemosphere* **2021**, *271*, 129810. [[CrossRef](#)] [[PubMed](#)]
14. Guan, R.P.; Yuan, X.Z.; Wu, Z.B.; Jiang, L.B.; Li, Y.F.; Zeng, G.M. Principle and application of hydrogen peroxide based advanced oxidation processes in activated sludge treatment: A review. *Chem. Eng. J.* **2018**, *339*, 519–530. [[CrossRef](#)]
15. Lee, J.; von Gunten, U.; Kim, J.H. Persulfate-Based Advanced Oxidation: Critical Assessment of Opportunities and Roadblocks. *Environ. Sci. Technol.* **2020**, *54*, 3064–3081. [[CrossRef](#)]
16. Lian, W.; Yi, X.; Huang, K.; Tang, T.; Wang, R.; Tao, X.; Zheng, Z.; Dang, Z.; Yin, H.; Lu, G. Degradation of tris(2-chloroethyl) phosphate (TCEP) in aqueous solution by using pyrite activating persulfate to produce radicals. *Ecotoxicol. Environ. Saf.* **2019**, *174*, 667–674. [[CrossRef](#)]
17. Li, Y.X.; Liu, L.; Li, W.; Lan, Y.Q.; Chen, C. Simultaneously rapid degradation of phenylphosphonic acid and efficient adsorption of released phosphate in the system of peroxy-monosulfate (PMS) and Co<sub>3</sub>O<sub>4</sub>-La<sub>2</sub>O<sub>3</sub>/C derived from MOFs. *J. Environ. Chem. Eng.* **2021**, *9*, 106332. [[CrossRef](#)]
18. Lominchar, M.A.; Rodriguez, S.; Lorenzo, D.; Santos, N.; Romero, A.; Santos, A. Phenol abatement using persulfate activated by nZVI, H<sub>2</sub>O<sub>2</sub> and NaOH and development of a kinetic model for alkaline activation. *Environ. Technol. Innov.* **2018**, *39*, 35–43. [[CrossRef](#)]
19. Lei, Y.; Chen, C.S.; Tu, Y.J.; Huang, Y.H.; Zhang, H. Heterogeneous Degradation of Organic Pollutants by Persulfate Activated by CuO-Fe<sub>3</sub>O<sub>4</sub>: Mechanism, Stability, and Effects of pH and Bicarbonate Ions. *Environ. Sci. Technol.* **2015**, *49*, 6838–6845. [[CrossRef](#)]
20. Pan, Y.W.; Zhou, M.H.; Zhang, Y.; Cai, J.J.; Li, B.; Sheng, X.J. Enhanced degradation of Rhodamine B by pre-magnetized Fe<sup>0</sup>/PS process: Parameters optimization, mechanism and interferences of ions. *Sep. Purif. Technol.* **2018**, *203*, 66–74. [[CrossRef](#)]
21. Li, H.J.; Fu, Y.H.; Mei, C.G.; Wang, M. Effective degradation of Direct Red 81 using FeS-activated persulfate process. *J. Environ. Manag.* **2022**, *308*, 114616. [[CrossRef](#)] [[PubMed](#)]
22. Zheng, H.; Bao, J.G.; Huang, Y.; Xiang, L.J.; Faheem; Ren, B.X.; Du, J.K.; Nadagouda, M.N.; Dionysiou, D.D. Efficient degradation of atrazine with porous sulfurized Fe<sub>2</sub>O<sub>3</sub> as catalyst for peroxy-monosulfate activation. *Appl. Catal. B* **2019**, *259*, 118056. [[CrossRef](#)]
23. Zhao, L.; Zhang, H.; Zhao, B.B.; Lyu, H.H. Activation of peroxydisulfate by ball-milled α-FeOOH/biochar composite for phenol removal: Component contribution and internal mechanisms. *Environ. Pollut.* **2022**, *293*, 118596. [[CrossRef](#)] [[PubMed](#)]
24. Xu, J.; Zhang, X.L.; Sun, C.; Wan, J.Z.; He, H.; Wang, F.; Dai, Y.X.; Yang, S.G.; Lin, Y.S.; Zhan, X.H. Insights into removal of tetracycline by persulfate activation with peanut shell biochar coupled with amorphous Cu-doped FeOOH composite in aqueous solution. *Environ. Sci. Pollut. Res.* **2019**, *26*, 2820–2834. [[CrossRef](#)] [[PubMed](#)]
25. Weng, H.; Yang, Y.; Zhang, C.; Cheng, M.; Wang, W.; Song, B.; Luo, H.; Qin, D.; Huang, C.; Qin, F.; et al. Insight into FeOOH-mediated advanced oxidation processes for the treatment of organic polluted wastewater. *Chem. Eng. J.* **2023**, *453*, 139812. [[CrossRef](#)]
26. Shi, T.S.; Jiang, F.; Wang, P.; Yue, T.; Sun, W. Deep purification of As(V) in drinking water by silica gel loaded with FeOOH and MnO<sub>2</sub>. *J. Cent. South Univ.* **2021**, *28*, 1692–1706. [[CrossRef](#)]
27. Chen, H.; Wang, J.L. MOF-derived Co<sub>3</sub>O<sub>4</sub>-C@FeOOH as an efficient catalyst for catalytic ozonation of norfloxacin. *J. Hazard. Mater.* **2021**, *403*, 123697. [[CrossRef](#)]
28. Ding, S.; Wan, J.Q.; Ma, Y.W.; Wang, Y.; Pu, M.J.; Li, X.T.; Sun, J. Water stable SiO<sub>2</sub>-coated Fe-MOF-74 for aqueous dimethyl phthalate degradation in PS activated medium. *J. Hazard. Mater.* **2021**, *411*, 125194. [[CrossRef](#)]
29. Ai, H.; Li, X.; Chen, C.; Xu, L.; Fu, M.-L.; Sun, W.; Yuan, B. Immobilization of β-FeOOH nanomaterials on the basalt fiber as a novel porous composite to effectively remove phosphate from aqueous solution. *Colloids Surf. A Physicochem. Eng. Asp.* **2022**, *632*, 127815. [[CrossRef](#)]
30. Zhao, L.J.; Ma, N.; Tao, M.L.; Zhang, W.Q. Covalently functionalized polyacrylonitrile fibers for heterogeneous catalysis and pollutant adsorption: A review. *Mater. Today Chem.* **2022**, *26*, 101206. [[CrossRef](#)]
31. Xu, G.; Wang, L.; Li, M.; Tao, M.; Zhang, W. Phosphorous acid functionalized polyacrylonitrile fibers with a polarity tunable surface micro-environment for one-pot C–C and C–N bond formation reactions. *Green Chem.* **2017**, *19*, 5818–5830. [[CrossRef](#)]

32. Xu, G.; Jin, M.; Kalkhaje, Y.K.; Wang, L.; Tao, M.; Zhang, W. Proton sponge functionalized polyacrylonitrile fibers as an efficient and recyclable superbasic catalyst for Knoevenagel condensation in Water. *J. Clean. Prod.* **2019**, *231*, 77–86. [[CrossRef](#)]
33. Xu, G.; Wang, L.; Xie, Y.J.; Tao, M.L.; Zhang, W.Q. Highly selective and efficient adsorption of Hg<sup>2+</sup> by a recyclable aminophosphonic acid functionalized polyacrylonitrile fiber. *J. Hazard. Mater.* **2018**, *344*, 679–688. [[CrossRef](#)] [[PubMed](#)]
34. Xu, G.; Xie, Y.J.; Cao, J.; Tao, M.L.; Zhang, W.Q. Highly selective and efficient chelating fiber functionalized by bis(2-pyridylmethyl)amino group for heavy metal ions. *Polym. Chem.* **2016**, *7*, 3874–3883. [[CrossRef](#)]
35. Xu, W.S.; Zheng, W.J.; Wang, F.J.; Xiong, Q.Z.; Shi, X.L.; Kalkhaje, Y.K.; Xu, G.; Gao, H.J. Using iron ion-loaded aminated polyacrylonitrile fiber to efficiently remove wastewater phosphate. *Chem. Eng. J.* **2021**, *403*, 126349. [[CrossRef](#)]
36. Zheng, W.J.; Wu, Q.W.; Xu, W.S.; Xiong, Q.Z.; Kalkhaje, Y.K.; Zhang, C.C.; Xu, G.; Zhang, W.F.; Ye, X.X.; Gao, H.J. Efficient capture of phosphate from wastewater by a recyclable ionic liquid functionalized polyacrylonitrile fiber: A typical “release and catch” mechanism. *Environ. Sci. Water Res. Technol.* **2022**, *8*, 607–618. [[CrossRef](#)]
37. Xu, G.; Xu, W.S.; Tian, S.; Zheng, W.J.; Yang, T.; Wu, Y.X.; Xiong, Q.Z.; Kalkhaje, Y.K.; Gao, H.J. Enhanced phosphate removal from wastewater by recyclable fiber supported quaternary ammonium salts: Highlighting the role of surface polarity. *Chem. Eng. J.* **2021**, *416*, 127889. [[CrossRef](#)]
38. Zhou, Q.; Wang, X.; Liu, J.; Zhang, L. Phosphorus removal from wastewater using nano-particulates of hydrated ferric oxide doped activated carbon fiber prepared by Sol–Gel method. *Chem. Eng. J.* **2012**, *200–202*, 619–626. [[CrossRef](#)]
39. Xu, G.; Cao, J.; Zhao, Y.L.; Zheng, L.S.; Tao, M.L.; Zhang, W.Q. Phosphorylated Polyacrylonitrile Fibers as an Efficient and Greener Acetalization Catalyst. *Chem. Asian J.* **2017**, *12*, 2565–2575. [[CrossRef](#)]
40. Zheng, L.S.; Li, P.Y.; Tao, M.L.; Zhang, W.Q. Regulation of polar microenvironment on the surface of tertiary amines functionalized polyacrylonitrile fiber and its effect on catalytic activity in Knoevenagel condensation. *Catal. Commun.* **2019**, *118*, 19–24. [[CrossRef](#)]
41. Grzybek, J.; Gil, B.; Roth, W.J.; Skoczek, M.; Kowalczyk, A.; Chmielarz, L. Characterization of Co and Fe-MCM-56 catalysts for NH<sub>3</sub>-SCR and N<sub>2</sub>O decomposition: An in situ FTIR study. *Spectrochim. Acta Part A* **2018**, *196*, 281–288. [[CrossRef](#)] [[PubMed](#)]
42. Zhang, G.; Fan, H.M.; Zhou, R.Y.; Yin, W.Y.; Wang, R.B.; Yang, M.; Xue, Z.Y.; Yang, Y.S.; Yu, J.X. Decorating UiO-66-NH<sub>2</sub> crystals on recyclable fiber bearing polyamine and amidoxime bifunctional groups via cross-linking method with good stability for highly efficient capture of U(VI) from aqueous solution. *J. Hazard. Mater.* **2022**, *424*, 127273. [[CrossRef](#)] [[PubMed](#)]
43. Lin, Z.; Yang, J.; Jia, X.H.; Li, Y.; Song, H.J. Polydopamine/FeOOH-modified interface in carbon cloth/polyimide composites for improved mechanical/tribological properties. *Mater. Chem. Phys.* **2020**, *243*, 122677. [[CrossRef](#)]
44. Zhu, H.; Xu, G.; Du, H.M.; Zhang, C.L.; Ma, N.; Zhang, W.Q. Prolinamide functionalized polyacrylonitrile fiber with tunable linker length and surface microenvironment as efficient catalyst for Knoevenagel condensation and related multicomponent tandem reactions. *J. Catal.* **2019**, *374*, 217–229. [[CrossRef](#)]
45. Guo, J.; Jiang, J.; Chen, Y.; Wen, X.; Chen, W.; Wang, Y.; Su, L.; Cao, J. Synthesis of nZVI-BC composite for persulfate activation to degrade pyrene: Performance, correlative mechanisms and degradation pathways. *Process Saf. Environ.* **2022**, *162*, 733–745. [[CrossRef](#)]
46. Meddah, S.; El Hadi Samar, M.; Bououdina, M.; Khezami, L. Outstanding performance of electro-Fenton/ultra-violet/ultra-sound assisted-persulfate process for the complete degradation of hazardous pollutants in contaminated water. *Process Saf. Environ.* **2022**, *165*, 739–753. [[CrossRef](#)]
47. Li, Y.; Zhao, X.; Yan, Y.; Yan, J.; Pan, Y.; Zhang, Y.; Lai, B. Enhanced sulfamethoxazole degradation by peroxymonosulfate activation with sulfide-modified microscale zero-valent iron (S-mFe<sup>0</sup>): Performance, mechanisms, and the role of sulfur species. *Chem. Eng. J.* **2019**, *376*, 121302. [[CrossRef](#)]
48. Wang, B.; Li, Q.; Lv, Y.; Fu, H.; Liu, D.; Feng, Y.; Xie, H.; Qu, H. Insights into the mechanism of peroxydisulfate activated by magnetic spinel CuFe<sub>2</sub>O<sub>4</sub>/SBC as a heterogeneous catalyst for bisphenol S degradation. *Chem. Eng. J.* **2021**, *416*, 129162. [[CrossRef](#)]
49. Yang, Q.; Wang, X.L.; Luo, W.; Sun, J.; Xu, Q.X.; Chen, F.; Zhao, J.W.; Wang, S.N.; Yao, F.B.; Wang, D.B.; et al. Effectiveness and mechanisms of phosphate adsorption on iron-modified biochars derived from waste activated sludge. *Bioresour. Technol.* **2018**, *247*, 537–544. [[CrossRef](#)]
50. Zhang, Y.; Tang, Q.; Sun, Y.F.; Yao, C.X.; Yang, Z.; Yang, W.B. Improved utilization of active sites for phosphorus adsorption in FeOOH/anion exchanger nanocomposites via a glycol-solvothermal synthesis strategy. *J. Environ. Sci.* **2022**, *111*, 313–323. [[CrossRef](#)]
51. Sun, H.M.; Zhou, Q.; Zhao, L.; Wu, W.Z. Enhanced simultaneous removal of nitrate and phosphate using novel solid carbon source/zero-valent iron composite. *J. Clean. Prod.* **2021**, *289*, 125757. [[CrossRef](#)]
52. Liu, F.L.; Zuo, J.E.; Chi, T.; Wang, P.; Yang, B. Removing phosphorus from aqueous solutions by using iron-modified corn straw biochar. *Front. Environ. Sci. Eng.* **2015**, *9*, 1066–1075. [[CrossRef](#)]
53. Brazão Farinha, C.; de Brito, J.; Veiga, R. Incorporation of high contents of textile, acrylic and glass waste fibres in cement-based mortars. Influence on mortars’ fresh, mechanical and deformability behaviour. *Constr. Build. Mater.* **2021**, *303*, 124424. [[CrossRef](#)]
54. Liu, H.; Bruton, T.A.; Doyle, F.M.; Sedlak, D.L. In Situ Chemical Oxidation of Contaminated Groundwater by Persulfate: Decomposition by Fe(III)- and Mn(IV)-Containing Oxides and Aquifer Materials. *Environ. Sci. Technol.* **2014**, *48*, 10330–10336. [[CrossRef](#)] [[PubMed](#)]
55. Wu, Y.; Prulho, R.; Brigante, M.; Dong, W.; Hanna, K.; Mailhot, G. Activation of persulfate by Fe(III) species: Implications for 4-tert-butylphenol degradation. *J. Hazard. Mater.* **2017**, *322 Pt B*, 380–386. [[CrossRef](#)]

56. Ma, X.; Yuan, H.; Qiao, Q.; Zhang, S.; Tao, H. Enhanced catalysis for degradation of rhodamine B by amino-functionalized Fe-MOFs with high adsorption capacity. *Colloids Surf. A Physicochem. Eng. Asp.* **2023**, *664*, 131099. [[CrossRef](#)]
57. Yang, T.-S.; Zhang, Y.; Cao, X.-Q.; Zhang, J.; Kan, Y.-J.; Wei, B.; Zhang, Y.-Z.; Wang, Z.-Z.; Jiao, Z.-Y.; Zhang, X.-X.; et al. Water caltrop-based carbon catalysts for cooperative adsorption and heterogeneous activation of peroxydisulfate for tetracycline oxidation via electron transfer and non-radical pathway. *Appl. Surf. Sci.* **2022**, *606*, 154823. [[CrossRef](#)]
58. Zhang, B.; Chen, N.; Feng, C.; Zhang, Z. Adsorption for phosphate by crosslinked/non-crosslinked-chitosan-Fe(III) complex sorbents: Characteristic and mechanism. *Chem. Eng. J.* **2018**, *353*, 361–372. [[CrossRef](#)]
59. Zhang, S.; Zhang, Y.; Ding, J.; Zhang, Z.; Gao, C.; Halimi, M.; Demey, H.; Yang, Z.; Yang, W. High phosphate removal using La(OH)<sub>3</sub> loaded chitosan based composites and mechanistic study. *J. Environ. Sci.* **2021**, *106*, 105–115. [[CrossRef](#)]
60. Li, X.; Elgarhy, A.H.; Hassan, M.E.; Chen, Y.; Liu, G.; Elkorashey, R.M. Removal of inorganic and organic phosphorus compounds from aqueous solution by ferrihydrite decoration onto graphene. *Environ. Monit. Assess.* **2020**, *192*, 1–9. [[CrossRef](#)]
61. Zhang, X.; Yao, H.; Lei, X.; Lian, Q.; Roy, A.; Doucet, D.; Yan, H.; Zappi, M.E.; Gang, D.D. A comparative study for phosphate adsorption on amorphous FeOOH and goethite ( $\alpha$ -FeOOH): An investigation of relationship between the surface chemistry and structure. *Environ. Res.* **2021**, *199*, 111223. [[CrossRef](#)] [[PubMed](#)]
62. Tao, R.; Qu, M.; Zhang, S.; Quan, F.; Zhang, M.; Shen, W.; Mei, Y. Preparation of FeOOH supported by melamine sponge and its application for efficient phosphate removal. *J. Environ. Chem. Eng.* **2022**, *10*. [[CrossRef](#)]
63. Wu, Z.-Y.; Zhao, H.; Hu, X.; Yuan, B.; Fu, M.-L. Tunable porous ferric composite for effective removal of phosphate in water. *Colloids Surfaces A: Physicochem. Eng. Asp.* **2019**, *582*, 123854. [[CrossRef](#)]
64. Harijan, D.K.; Chandra, V. Akaganeite nanorods decorated graphene oxide sheets for removal and recovery of aqueous phosphate. *J. Water Process. Eng.* **2017**, *19*, 120–125. [[CrossRef](#)]
65. Zhang, X.; Gang, D.D.; Sun, P.; Lian, Q.; Yao, H. Goethite dispersed corn straw-derived biochar for phosphate recovery from synthetic urine and its potential as a slow-release fertilizer. *Chemosphere* **2020**, *262*, 127861. [[CrossRef](#)]

**Disclaimer/Publisher's Note:** The statements, opinions and data contained in all publications are solely those of the individual author(s) and contributor(s) and not of MDPI and/or the editor(s). MDPI and/or the editor(s) disclaim responsibility for any injury to people or property resulting from any ideas, methods, instructions or products referred to in the content.